Biosynthesis of NiO-NPs using mucilage of *Cordia myxa* fruit and their potential application as an efficient catalyst for the synthesis of chromenes

Fatemeh Mirsalari[1] · Elham Tahanpesar[1] · Haleh Sanaeishoar[1]

Abstract

In the present study, a novel biosynthetic process of NiO-NPs is described using an economical reducing/capping agent (*Cordia myxa* fruit mucilage) by the simple sol–gel method, and $Ni(NO_3)_2.6H_2O$ as a nickel precursor. The nanoparticles were calcinated at different temperatures of 500, 600, and 700 °C. The structure, size, and morphology of these nanoparticles were characterized by FT-IR, XRD, FESEM, and EDS spectroscopy. The thermal manner of the composition has been studied by the utilization of TGA. Analyses of XRD verified that the pure and single-crystalline phase of NiO-NPs was formed when the sample was calcinated at 700 °C. The average particle size of 15 to 27 nm was obtained which showed that increasing the calcination temperature could lead to an increase in the size of NiO-NPs. The result from FESEM revealed that nanoparticles were uniformly distributed while being homogenous and nearly spherical as well. Further, NiO-NPs showed excellent catalytic activity through a three-component condensation reaction for the synthesis of 3,4-dihyropyrano[*c*]chromenes and 2-amino-4H-chromene derivatives. This effective catalyst could be recovered and reused several times without any significant loss of activity.
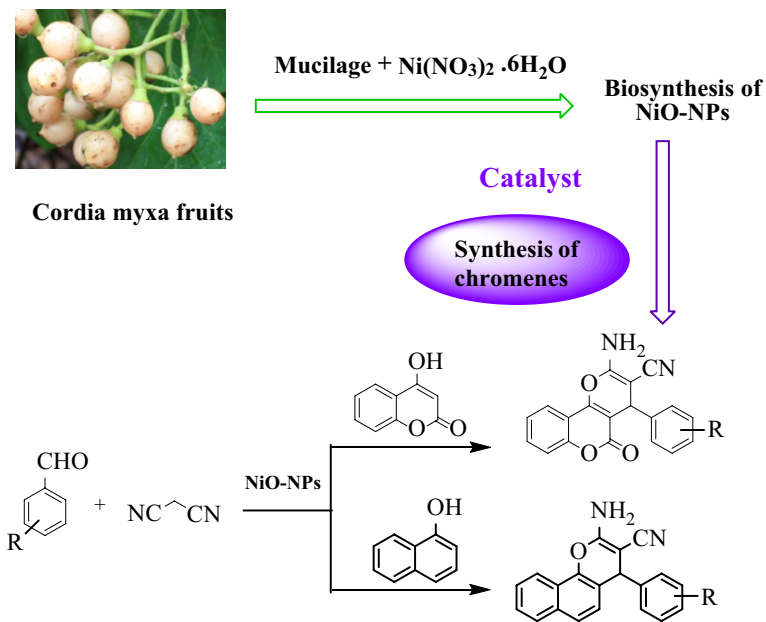
✉ Elham Tahanpesar
  Etahanpesar@iauahvaz.ac.ir; Tahanpesar@yahoo.com

  Fatemeh Mirsalari
  f.mirsalari63@gmail.com

  Haleh Sanaeishoar
  halehsanaei@yahoo.com

[1] Department of Chemistry, Ahvaz Branch, Islamic Azad University, Ahvaz, Iran

Graphical abstract

Keyword NiO nanoparticles · Biosynthesis · *Cordia myxa* mucilage · Chromenes

Introduction

Nowadays, nano-scaled materials have received steadily growing attention as a result of their peculiar and fascinating properties and applications superior to their bulk counterparts. A key factor in the behavior of nanomaterials is the size and shape of nanoparticles. The various parameters such as type of precursors, stabilizing agents, concentrations of precursors, pH value and calcination temperature, etc. affect the morphology and size of pure nanoparticles [1].

Therefore, considering the effect of the shape and size of particles on the chemical and physical properties of materials, the necessity of trying to achieve new methods to produce nanocrystals with controllable size and morphology is important for researchers. Among the various nanomaterials, metal oxides have attracted many researchers since they contain amazing features, such as being catalytic, magnetic, electrical, and optical, along with general qualities such as thermal stability and chemical passivity [2–4].

Nickel oxide nanoparticles (NiO-NPs) are black solid, inorganic compounds and one of the most important metal oxides, that are insoluble in all solvents and can be attacked by base and acid [5]. NiO-NPs are highly considered due to their

applications in various fields such as catalysis [6], sensors [7], and biomedical and materials science [3].

Much research has been done on the synthesis process and photocatalytic, cytotoxicity, magnetic, and antibacterial activity of NiO nanoparticles, but a survey of the literature revealed that the biosynthetic process of NiO-NPs by the sol–gel method, using *Cordia myxa* fruit mucilage as a reducing and capping agent has never been reported.

Conventionally, nanoparticles were synthesized by different chemical methods such as the sol–gel technique and chemical reduction. But these methods employ the use of toxic chemicals and also result in the production of hazardous side products. Thus, there always remains a quest in the scientific community to develop methods that are less toxic, eco-friendly, cost-effective, and clean for the synthesis of nanoparticles [8]. Using plants for the synthesis of metal oxide nanoparticles has drawn attention in recent years because of its eco-friendly, reduced chemical utilization, and simple experimental setup for the biosynthetic process [9].

Plants contain many natural compounds such as flavonoids, polysaccharides, saponins, alkaloids, polyphenols, and tannins, which are secondary metabolites that act as both natural reducing and capping agents in the biosynthesis process of nanoparticles [10–14]. These natural products are derived from different parts of the plant such as leaves, stems, roots, flowers, fruits, and seeds. One of these natural compounds that are extracted from some plants is mucilage. Mucilages are polysaccharides formed by large molecules of sugars and uronic acids joined together by glycosidic links [15]. It also contains proteins, minerals, lipids, tannins, phenolic compounds, alkaloids, and steroids, as well as monosaccharides produced by hydrolysis [16].

Green synthesis of metal oxide nanoparticles using natural polysaccharide compounds such as okra [9, 17], chia [18, 19], and Cydonia oblong seeds mucilage [5, 20], Arabic and tara gum [21, 22], the leaf extract of Rhamnus virgate and starch [23–25] have already been reported. Ankamwar et al. reported the green synthesis of gold nanoparticles from the aqueous *Cordia myxa* fruit extract, which could serve as the source for both the reducing and stabilizing agents [26].

Cordia myxa is a mid-sized deciduous tree belonging to the borage family (Boraginaceae). This plant has extraordinary pharmacological and biological properties. The phytochemical studies have revealed the presence of carbohydrates, glucose, flavonoids, sterols, saponins, terpenoids, alkaloids, phenolic acids, and mucilage plentiful in *Cordia myxa* [27]. Previously the total phenolic content, antioxidant activity, and functional properties of *Cordia myxa* mucilage have been investigated by Keshani Dokht et al. showing good phenolic content in the mucilage [28]. Furthermore, it has been reported that *Cordia myxa* mucilage can be used as a matrix for making nanoparticles [28].

The enhanced surface-area-to-volume ratio in nanoparticles makes them excellent for use as catalysts, in chemical reactions [29, 30]. Among these catalysts, metal oxides have emerged as a new class of heterogeneous nanocatalysts for organic transformations and organic synthesis. Compared to homogeneous catalysts, heterogeneous ones have advantages such as easy separation, recyclability, low cost, ease of handling, and minimization of waste products [31].
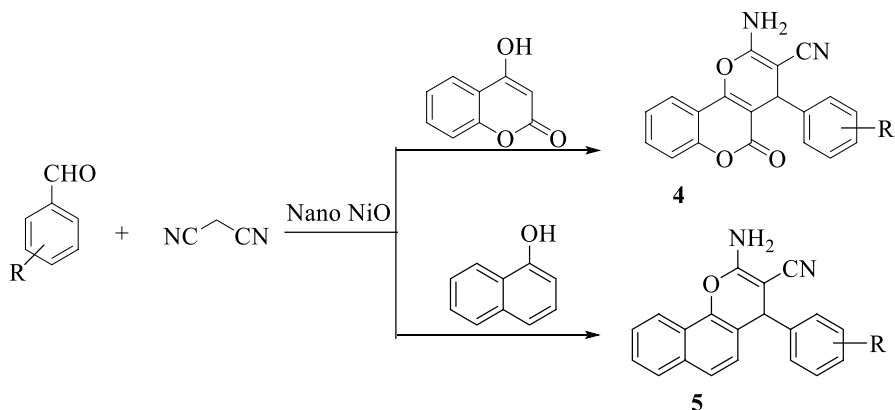
Scheme 1 Preparation of 3,4-dihydropyrano[*c*]chromene (**4**) and 2-amino-4H-chromene (**5**)derivatives using NiO-NPs

Choromene derivatives are an important group of heterocyclic compounds. In addition, 2-amino-4H-chromene and 3,4-dihyropyrano[*c*]chromenes and their derivatives are very useful compounds in various fields of chemistry, pharmacology, and biology [32]. Some of these compounds exhibit spasmolytic [33], anticancer, anticoagulant [34], and anti-anaphylactic activity [35, 36].

Recently, several methods have been reported for the synthesis of 3,4-dihyropyrano[*c*]chromene derivatives in the presence of various catalysts such as MgO, ZnO, $CuCr_2O_4$, Fe_3O_4@SiO_2-Imine/Phenoxy-Cu(II) and CuO nanoparticle[37–39]. In this article, we have reported for the first time the biosynthetic process of NiO nanoparticles by the mucilage of *Cordia myxa* fruit, which can act as the source of both reducing and capping agents. The nanoparticles were calcinated at different temperatures of 500, 600, and 700 °C, thus the influence of temperature was also Investigated. The biosynthesized NiO nanoparticles were characterized by the X-ray diffraction method (XRD), Fourier transforms infrared spectroscopy (FT-IR), Field emission scanning electron microscopy (FESEM), and the application of TGA. In continuation of our interests to develop environmentally benign protocols, we decided to use synthesized NiO-NPs as a catalyst for the preparation of 3,4-dihydropyrano[*c*]chromenes (**4**) and 2-amino-4H-chromene derivatives (**5**) by three-component condensation reaction (Scheme 1).

Experimental

Chemicals and apparatus

Nickel nitrate hexahydrate, $Ni(NO_3)_2.6H_2O$ was purchased from Merck Chemical Company with a purity of over 99%. Fresh *Cordia myxa* fruits were collected from plants growing in local areas of Khuzestan province, Iran. All reagents and solvents for synthesis were analytical grades and double distilled water was used throughout

the experiments. FT-IR spectra were recorded on AVATAR- Thermo, and Perkin-Elmer (RX 700) FT-IR spectrophotometers as KBr pellets. The crystallinity of the catalyst was investigated by Holland Philips Xpert X-ray powder diffraction (XRD) (Cu Kα, radiation, k $=0.154056$ nm), from 10 to 80° (2θ). The surface morphology of the catalyst was characterized by a FESEM, TESCAN MIRA III FESEM equipped with side detectors of EDS, and high-resolution elemental mapping to detect elemental compositions. The TGA was conducted on a Linseis (SDT Q600 V20.9 Build 20) thermogravimetric analyzer with a heating rate of 10 °C min^{-1} from 20 to 800 °C of in an air atmosphere. Monitoring of the reaction was fulfilled by TLC on silica gel polygram SILG/UV 254 plates. The synthesized compounds were characterized by ^{1}H and ^{13}C NMR spectra on a Bruker DRX-250 spectrometer. The melting points were determined using an Electrothermal melting point apparatus by the open capillary tube method and were uncorrected.

Preparation of mucilage of *Cordia myxa* fruit

To prepare the mucilage, first, the fresh fruits of *Cordia myxa* (50.0 g) were washed with water and then added to 100 ml of distilled water that was placed at room temperature for 24 h. Then it was heated for 30 min. at 50–60 °C. Finally, the obtained mucilage is filtered and stored in the refrigerator for further use [17].

Synthesis of NiO nanoparticles using mucilage of *Cordia myxa* fruit

For the fabrication of nickel oxide NPs, 5 g Ni(NO$_3$)$_2$.6H$_2$O powder was added to 100 ml mucilage and then the obtained solution was stirred in an oil bath for 4 h at a constant temperature of 80 °C with a magnetic stirrer. The green and sticky gel was finally achieved at the bottom of the beaker. This remaining product was dried in an oven at 120 °C for 12 h and divided into 3 parts. In the last step, calcination is performed at temperatures of 500, 600, and 700 °C for 4 h to obtain a black powder, which is known as NiO-NPs. The applied biosynthesis plan of our product is exhibited in Fig. 1.

General procedure for the synthesis of 3,4-dihydropyrano[*c*]chromenes and 2-amino-4H-chromene derivatives using NiO-NPs

A mixture of an aromatic aldehyde (1 mmol), malononitrile (1.2 mmol), 4-hydroxy coumarin (1 mmol, for compounds **4**) or 1-naphthol (1 mmol, for compounds **5**), and NiO NPs (0.02 g) in 5 ml water was taken in a round bottom flask. The reaction mixture was stirred at 80 °C and the progress of the reaction was followed by TLC using n-hexane: ethyl acetate (3: 1). After completion of the reaction, the reaction mixture was filtered to separate the catalyst. Finally, the evaporation was carried out to concentrate the residue of the solvent then the solid obtained was washed several times with ethanol. The purification of desired products was accomplished by recrystallization with hot ethanol. The structure of the products was determined based on their ^{1}H NMR, ^{13}C NMR, and IR spectra.
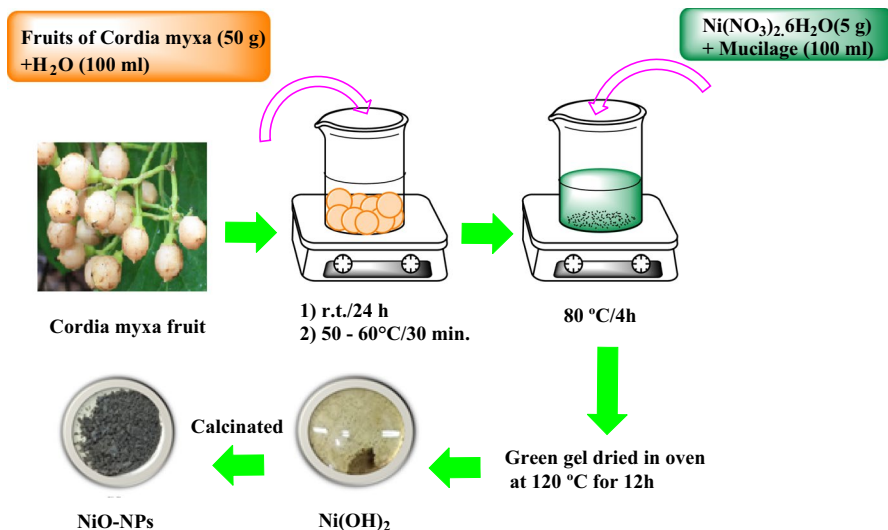
Fig. 1 Plan of the biosynthesis of NiO-NPs

Selected spectral data of the products

2-amino-4-(phenyl)-5-oxo-4,5-dihydropyrano[3,2-c]chromene-3-carbonitrile (4a), Yield 85%, White solid, Molecular formula $C_{19}H_{12}N_2O_3$, m.p = 257–259 °C; IR (KBr): 3379- 3284, 3178, 2197, 1708, 1674, 1606, 1382, 1057 cm^{-1}; ^{1}HNMR (250 MHz, DMSO-d$_6$) δ = 4.42 (s, 1H, benzylic–CH), 7.35 (s, 2H, NH$_2$), 7.41–7.90 (m, 9H, Ar–H) ppm; ^{13}C NMR (250 MHz, DMSO-d$_6$) δ 40.01, 59.51, 105.48, 114.43, 118.01, 120.61, 123.93, 126.11, 128.55, 129.05, 129.95, 134.37, 144.76, 153.61, 154.88, 159.46, 160.97 ppm.

2-amino-4-(3-bromophenyl)-5-oxo-4,5-dihydropyrano[3,2-c]chromene-3-carbonitrile (4b), Yield 90%, White solid, Molecular formula $C_{19}H_{11}BrN_2O_3$, m.p = 278–279 °C; IR (KBr): 3396, 3321, 3195, 2202, 1706, 1672, 1602, 1607, 1381, 1305, 1209,1053, 761 cm^{-1}; ^{1}HNMR (250 MHz, DMSO-d$_6$): δ 4.46 (s, 1H, benzylic–CH), 7.35 (s, 2H, NH$_2$), 7.41–7.87 (m, 8H, Ar–H) ppm; ^{13}C NMR (250 MHz, DMSO-d$_6$) δ 40.34, 58.93, 104.65, 114.40, 117.96, 120.46, 123.16, 124.00, 126.04, 128.37, 131.52, 131.87, 132.11, 134.39, 147.44, 153.65, 155.16, 159.48, 160.97 ppm.

2-amino-4-(2-chlorophenyl)-5-oxo-4,5-dihydropyrano[3,2-c]chromene-3-carbonitrile (4c), Yield 90%, White solid, Molecular formula $C_{19}H_{11}ClN_2O_3$, m.p = 267–269 °C; IR (KBr): 3399, 3383, 3178, 2199, 1709, 1674, 1601, 1380, 1258, 1212, 1172, 1111, 1061, 755 cm^{-1}, ^{1}HNMR (250 MHz, DMSO-d$_6$) δ 4.95 (s, 1H, benzylic–CH), 7.26 (s, 2H, NH$_2$), 7.27–7.90 (m, 8H, Ar–H) ppm; ^{13}C NMR (250 MHz, DMSO-d$_6$) δ 40.34, 160.81, 159.60, 155.49, 153.66, 141.63, 134.45, 133.89, 132.10, 131.03, 130.23, 129.12, 126.13, 123.69, 120.20, 118.03, 114.28, 104.36, 58.05 ppm.

2-amino-4-(4-nitrophenyl)-5-oxo-4,5-dihydropyrano[3,2-c]chromene-3-carbonitrile (4d), Yield 95%, Yellow solid, Molecular formula $C_{19}H_{11}N_3O_5$, m.p = 257–259 °C; IR (KBr): 3397, 3319, 3193, 2193, 1673, 1602, 1456, 1353,1377, 1062, 823 cm^{-1},^{1}HNMR (250 MHz, DMSO-d$_6$) δ 4.95 (s, 1H, benzylic–CH), 5.40 (s, 2H, NH$_2$), 7.34–7.90 (m, 8H, Ar–H) ppm; ^{13}C NMR (250 MHz, DMSO-d$_6$) δ 32.67, 36.64, 102.79, 109.73, 114.65, 121.45, 122.2, 129.94, 134.65, 146.74, 146.86, 148.02, 150.02, 150.50, 150.62, 167.42, 194.84 ppm.

2-amino-4-(4-cyanophenyl)-5-oxo-4,5-dihydropyrano[3,2-c]chromene-3-carbonitrile (4e), Yield 95%, White solid, Molecular formula $C_{20}H_{11}N_3O_3$, m.p = 282–285 °C; IR (KBr): 3613, 3431, 3322, 3055, 2234, 2197, 1456, 1718, 1672, 1598, 1491, 1456, 1372, 1303, 1272, 1256, 1212, 1171, 837 cm^{-1}, ^{1}HNMR (250 MHz, DMSO-d$_6$) δ 6.58 (s, 1H, benzylic–CH), 6.79 (s, 2H, NH$_2$), 7.60–7.92 (dd, *J* = 1.2; 1.6 HZ 8H, Ar–H) ppm; ^{13}C NMR (250 MHz, DMSO-d$_6$) δ 28.36, 59.08, 108.98, 109.09, 111.00, 111.67, 116.25, 121.77, 128.49, 130.70, 132.19, 133.96, 138.48, 147.59, 154.73, 159.65, 167.36,194.82 ppm.

2-amino-4-(4-chlorophenyl)-5-oxo-4,5-dihydropyrano[3,2-c]chromene-3 carbonitrile (4f), Yield 92%, White solid, Molecular formula $C_{19}H_{11}ClN_2O_3$, m.p = 259–260 °C; IR (KBr): 3379, 3296, 2192, 1712, 1676, 1377, 1094, 827 cm^{-1}.

2-amino-4-(4-hydroxyphenyl)-5-oxo-4,5-dihydropyrano[3,2-c]chromene-3-carbonitrile (4 g), Yield 85%, White solid, Molecular formula $C_{19}H_{12}N_2O_4$, m.p = 264–267 °C; IR (KBr): 3385, 3291, 2191, 1710, 1676, 1602, 1376, 1212, 1172, 1113, 1063, 975, 835, 759 cm^{-1}.

2-amino-4-(phenyl)-4H-benzo[h]chromene-3-carbonitrile (5a), Yield 80%, White solid, Molecular formula $C_{20}H_{14}N_2O$, m.p = 210–212 °C; IR (KBr): 3425, 3362, 2222, 1624, 1568, 1449, 1119 cm^{-1}.

2-amino-4-(4-nitrophenyl)-4H-benzo[h]chromene-3-carbonitrile (5d), Yield 95%, White solid, Molecular formula $C_{20}H_{13}N_3O_3$, m.p = 235–238 °C; IR (KBr): 3459, 3361, 2187, 1574, 1633, 1406, 1104,1513, 1345 cm^{-1}, ^{1}HNMR (250 MHz, DMSO-d$_6$) δ 5.12 (s, 1H, benzylic–CH), 7.08 (s, 1H, ArH), 7.29 (s, 1H, ArH), 7.87 (s, 2H, NH$_2$), 7.53 (d, 5H, *J* = 16.5 Hz, ArH), 8.18 (s, 3H, Ar–H) ppm; ^{13}C NMR (250 MHz, DMSO-d$_6$) δ 55.59, 117.06, 120.60, 121.18, 123.18, 124.53, 124.66, 126.37, 127.29, 127.49, 128.19, 129.48, 133.34, 143.36, 146.93, 153.42, 160.76 ppm.

2-amino-4-(4-chlorophenyl)-4H-benzo[h]chromene-3-carbonitrile (5f), Yield 85%, White solid, Molecular formula $C_{20}H_{13}ClN_2O$, m.p = 231–232 °C; IR (KBr): 3454, 3335, 2191, 1600, 1572, 1412, 1104,1013 cm^{-1}, ^{1}HNMR (250 MHz, DMSO-d$_6$) δ 4.92 (s, 1H, benzylic–CH), 7.58 (s, 2H, NH$_2$), 7.05 (d, 2H, *J* = 8 Hz, ArH), 7.17–7.37 (m, 6H, Ar–H) ppm; 7.85 (d, 1H, *J* = 7.25 Hz, ArH) 8.17 (d, 1H, *J* = 7.25 Hz, ArH) ^{13}C NMR (250 MHz, DMSO-d$_6$) δ 56.27, 117.84, 120.79, 121.15, 123.16, 124.46, 126.51, 127.18, 127.32, 128.14, 129.13, 130.01, 131.97, 133.19, 143.18, 145.10, 160.59 ppm.

2-amino-4-(4-hydroxyphenyl)-4H-benzo[h]chromene-3-carbonitrile (5 g), Yield 85%, White solid, Molecular formula $C_{20}H_{14}N_2O_2$, m.p = 187–188 °C; IR (KBr): 3439, 3350, 2226, 1611, 1566, 1445, 1174 cm^{-1}.

2-amino-4-(4-(dimethylamino)phenyl)-4H-benzo[h]chromene-3-carbonitrile (5 h), Yield 85%, White solid, Molecular formula $C_{22}H_{19}N_3O$, m.p = 200–202 °C;

IR (KBr): 3422, 3361, 2209, 1613, 1567, 1418, 1178 cm^{-1}, ^{1}HNMR (250 MHz, DMSO-d$_6$) δ 3.30 (s, 6H, Me), δ 5.13 (s, 1H, benzylic–CH), 8.03 (s, 2H, NH$_2$), 6.82 and 7.80 (d, $J = 10$ Hz and d, $J = 2.5$ Hz, 10H, ArH), ^{13}C NMR (250 MHz, DMSO-d$_6$) δ 40.11, 69.06, 112.27, 115.99, 116.73, 119.18, 122.70, 122.85, 124.06, 128.19, 128.03, 128.99, 129.04, 130.99, 133.52, 134.05, 154.78, 159.33 ppm.

2-amino-4-(4-bromophenyl)-4H-benzo[h]chromene-3-carbonitrile (5i), Yield 92%, White solid, Molecular formula C$_{20}$H$_{13}$BrN$_2$O, m.p = 232–235 °C; IR (KBr): 3471, 3330, 2195, 1601, 1577, 1409, 1103, 1070 cm^{-1}.

Results and discussion

Possible mechanism of formation of NiO nanoparticles

The mucilage of *Cordia myxa* fruit contains the secondary metabolites of polysaccharides and polyphenols [27]. The mechanism of biosynthesis of nickel oxide nanoparticles using mucilage is shown in Fig. 2. In the first step or nucleation stage, polysaccharides have an essential role as weak base sources to provide (OH^{-}) for hydrolyzing the nickel metal ions (nickel precursor) to form colloids of Ni(OH)$_n$. Then in the growth stage, the adjacent small nanoparticles become larger nanoparticles. Therefore, the metabolites present in the mucilage act as capping agents to prevent the agglomeration of nickel oxide nanoparticles. [18, 22]. In the final stage or stabilization stage, which determines the final shape of the nanoparticles, the calcination process is used [13, 40].
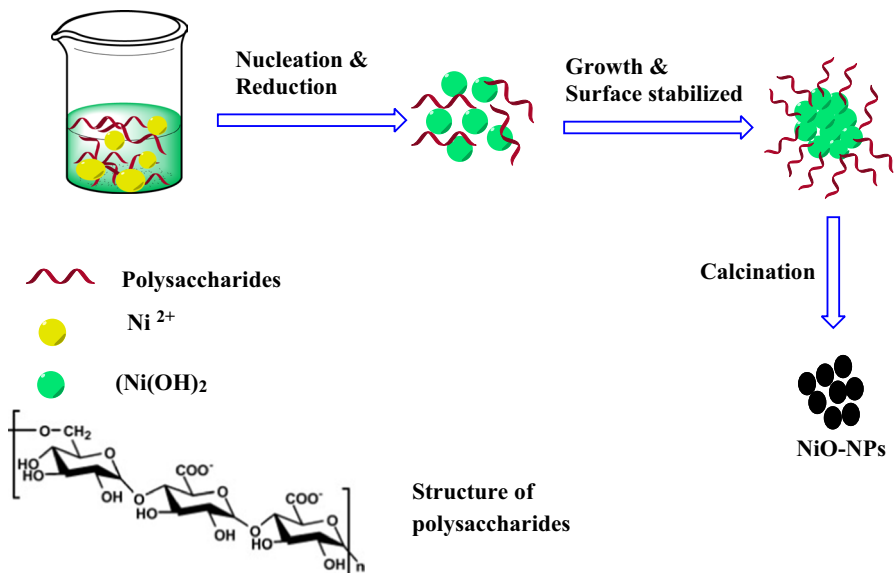
Fig. 2 The mechanism of biosynthesis of NiO-NPs using *Cordia myxa* mucilage

Characterization of NiO-NPs synthesized using mucilage of *Cordia myxa* fruit

FT-IR analysis

FT-IR analysis was performed to find out the different functional groups that are present in the mucilage of *Cordia myxa* fruit, and the synthesized nanoparticles.

FT-IR spectrum of the mucilage of *Cordia myxa* fruit is shown in Fig. 3. The peak observed at 3493 cm^{-1} is associated with a stretching vibration of OH alcoholic groups illustrating that *Cordia myxa* fruit contained the secondary metabolites of polysaccharides and flavonoids [41]. The low broadband at 3298 cm^{-1} could be due to water content [42]. The peak at 1631 cm^{-1} corresponded to carboxyl group stretching vibration, which was caused by the uronic acid component [43]. The observed signals between 950 and 1200 cm^{-1} refer to the stretching vibration of alcoholic C–O in COH bands in carbohydrates [28]. The signals observed at 628 and 739 cm^{-1} refer to the stretching vibration of C-H aromatic polyphenols extracted with mucilage from *Cordia myxa* fruit [27, 41].

The FT-IR spectra of synthesized NiO nanoparticles using mucilage of *Cordia myxa* fruit that has been calcinated at the temperatures of 500, 600, and 700 °C is also shown in Fig. 4. The broad band at 3419 cm^{-1} corresponded to the O–H stretching vibration of water molecules absorbed on the surface of samples or KBr. The bending vibration of this bond has been observed at 1637 cm^{-1}. The band at 1384 cm^{-1} is due to the presence of N=O stretching frequency induced by a trace amount of nitrate. The absorption band in the range of 420–500 cm^{-1} could be related to the Ni–O stretching vibration bands in NiO-NPs [3].
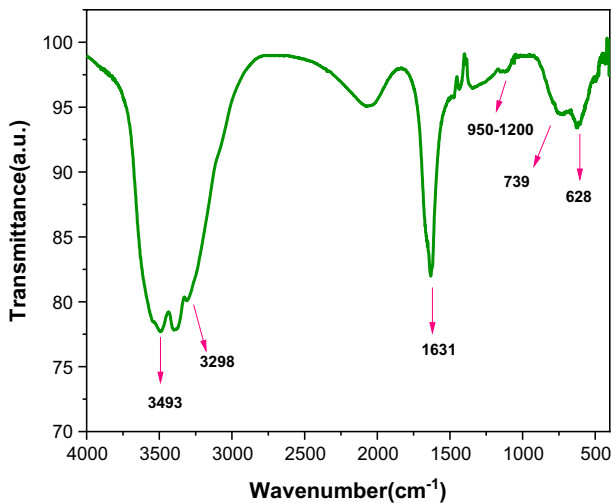

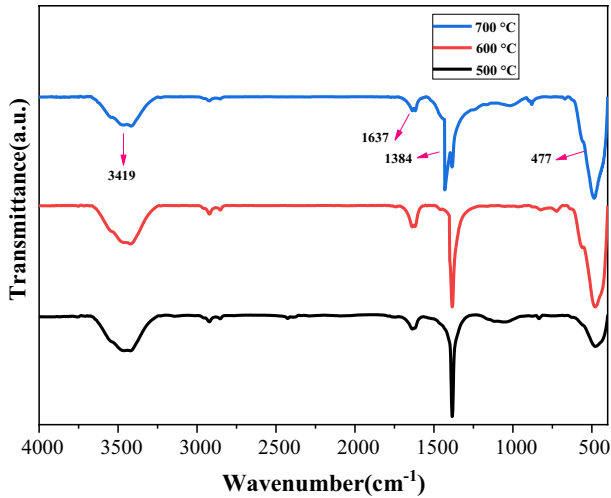**Fig. 3** FT-IR spectrum of mucilage of *Cordia myxa* fruit

Fig. 4 FT-IR spectra of NiO-NPs samples synthesized using mucilage of *Cordia myxa* fruit at different temperatures

XRD analysis

The X-ray diffraction patterns of the prepared NiO samples are presented in Fig. 5. In all samples, five different peak types at 2θ values of 37°, 43°, 63°, 75°, and 79° were corresponding to the (111), (200), (220), (311), and (222) respectively which suggests that the face-centered cubic (fcc) NiO–NPs contain a cubic crystal structure and matched very well with the reported values (JCPDS card no
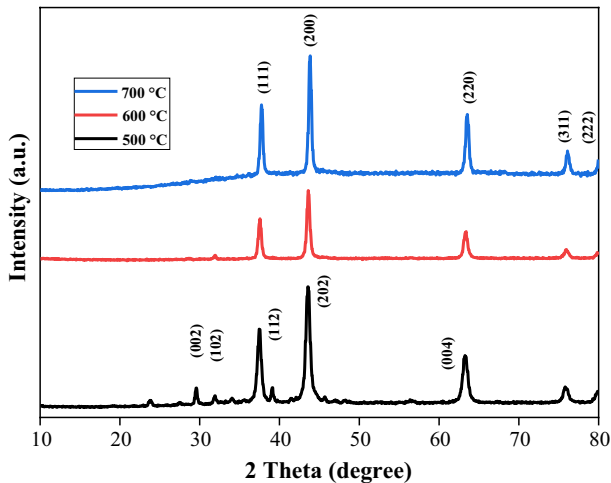
Fig. 5 XRD patterns of NiO–NPs synthesized using mucilage of *Cordia myxa* fruit at different temperatures

73–1519) [44]. The diffraction peaks at 2θ values at 28°, 31°, 41°, 45°, and 56° corresponding to the (002), (102), (112), (202), and (004) can be indexed to the planes of the Ni_2O_3 phase (JCPDS card no. 14–0481) when sample calcinated at 500 °C [45]. The XRD spectrum of nickel oxide calcinated at 600 and 700 °C has the pure phase of NiO and it is also observed that 700 °C has the highest peak intensity and degree of crystallinity.

The particle size has been estimated using the Debye–Scherrer formula: $D = K\lambda/\beta \cos\theta$, where D is the particle size (nm); K = 0.9 stands as the fixed number; λ would be the Cu Kα radiation wavelength (0.154 nm); β, represents the full-width at half maximum of the diffraction lines (rad), and θ, Bragg angle (degree). As listed in Table 1, the crystal sizes measured to be about 15–27 nm.

As can be seen from Fig. 5. increasing calcination temperature resulted in heightening the intensity of peaks and decreasing their width. An increase in the intensity of the peaks indicates an increase in the degree of crystallinity of the nanoparticles while a decrease in the width of the peaks specifies an increase in the size of the crystalline particles that can be caused by the particle joining and their growth at high temperatures [22, 46].

TGA analysis

The thermal behavior of a dried gel sample of mucilage was investigated using TGA analysis within an air atmosphere at the speed of 10 °C/min at a temperature range of 30–800 °C, which is displayed in Fig. 6. The TGA graph of the initial dry gel ($Ni(OH)_2$) using mucilage displayed the occurrence of weight loss in four stages. The initial weight loss of about 7% happened from 93 to 162 °C, which is associated with the removal of moisture content [47]. The second and third stages of weight loss reported to be 26% and 9%, occurred in the temperature range of 162–310 °C and 310–347.17 °C, respectively. These losses were attributed to the removal of hydroxyl groups of $Ni(OH)_2$ during the formation of NiO phases and the degradation of organic compounds [3, 48]. The last stage of small weight loss occurs at a temperature range of 400–800 °C, which is due to the generation of pure NiO phases. The TGA curve of nickel hydroxide gel obtained using mucilage is shown in Fig. 6.

Table 1 Effect of the calcination temperature for the synthesis of NiO-NP samples

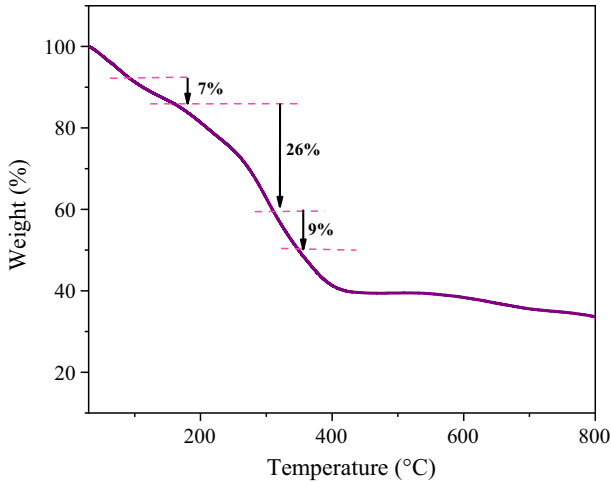| Calcination Temperature (°C)	2θ (°)	FWHM (rad)	Particle size (nm)	Composition of the product
500	43.6	0.5300	15	$NiO + Ni_2O_3$ (minor)
600	43.7	0.3936	21	NiO
700	43.8	0.2952	27	NiO

Fig. 6 TGA curve of nickel hydroxide gel obtained using mucilage

FESEM/EDS analysis

The morphological characteristics of the as-synthesized sample of NiO-NPs that was calcinated at 700 °C were studied by FESEM. Figure 7a–c displays images of NiO-NPs in different magnifications. Accordingly, the morphology of particles was uniformly distributed while being homogenous and nearly spherical as well [3]. The surface elemental distribution of the sample was examined by FESEM-EDS mapping (Fig. 8) which indicates the sample consists of Ni and O, with homogeneous distributions. The EDX analysis of the sample revealed Ni and O as significant elements (Fig. 9).
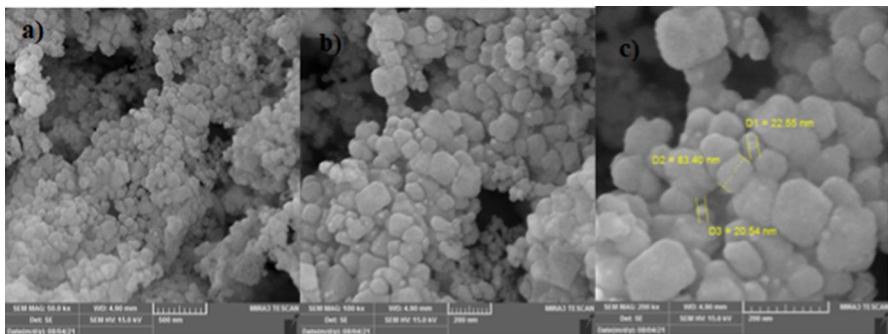
Fig. 7 FESEM images of NiO nanoparticles calcinated at 700 °C
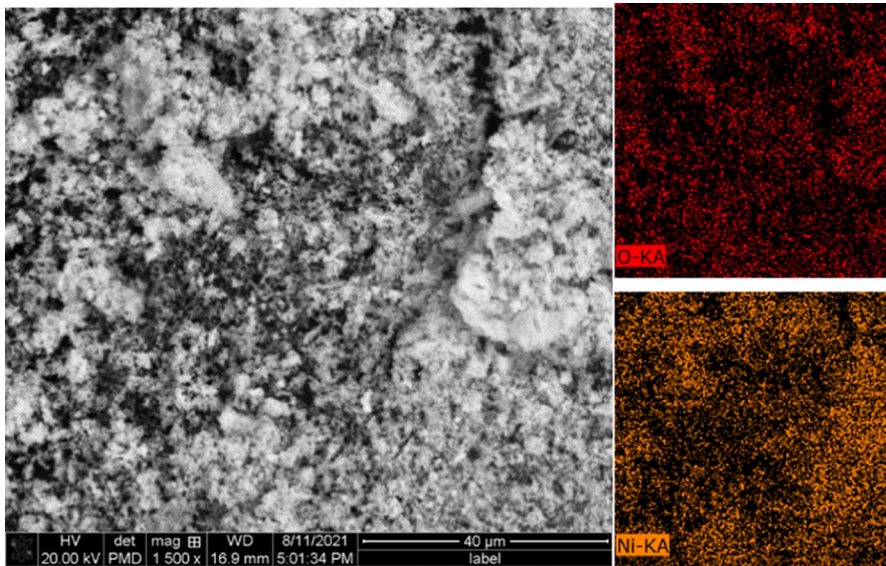
Fig. 8 Elemental mappings for NiO nanoparticles calcinated at 700 °C
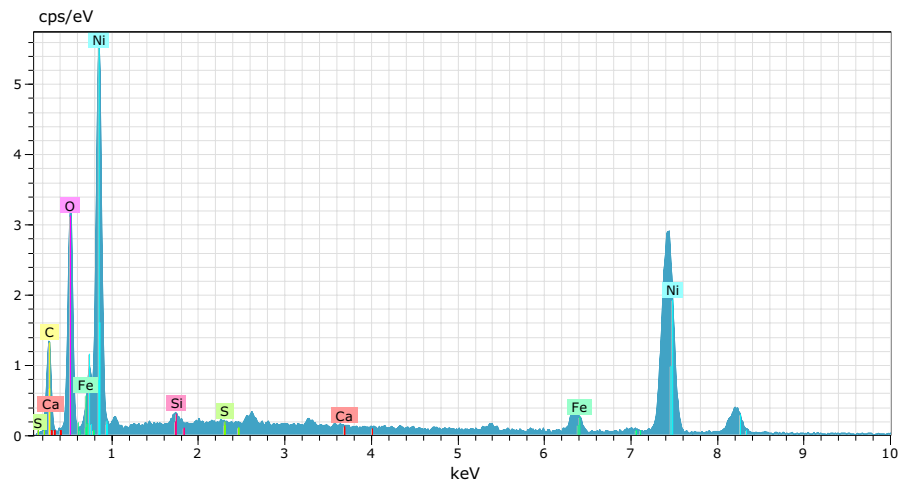
Fig. 9 EDX analysis of NiO nanoparticles calcinated at 700 °C

Catalytic studies

In general, a set of experiments was carried on by using the mucilage of *Cordia myxa* fruit as a reducing/capping agent and $Ni(NO_3)_2.6H_2O$ as a nickel precursor, by the sol–gel method. To obtain the optimal calcination temperature, the dried gel was divided into three parts which were calcinated at different temperatures of 500, 600, and 700 °C for 4 h and NiO-NPs were successfully formed.

The structure and size of these nanoparticles were characterized by FT-IR and XRD techniques (Figs. 4 and 5). The appearance of the absorption band in the range of 420–500 cm^{-1} which could be related to the Ni–O stretching vibration bands, revealed the formation of NiO-NPs in all samples at different temperatures (Fig. 4).

Employing the XRD technique to specify the crystal structure, grain size, crystalline phases, and purity of NiO-NP samples, showed the crystal sizes about 15–27 nm (Fig. 5, Table 1). XRD pattern of NiO showed NiO crystalline phase with lower purity due to the existence of the planes of the Ni_2O_3 phase, when the sample calcinated at 500 °C. Comparing the XRD spectrum of nickel oxide calcinated at 600 and 700 °C indicates the pure phase of NiO in both samples. Increasing calcination temperature from 600 to 700 °C resulted in heightening the intensity of peaks and decreasing their width. An increase in the intensity of the peaks indicates an increase in the degree of crystallinity [46].

Since the pure and single-crystal NiO phase resulted in the highest peak intensity and degree of crystallinity when a sample was calcined at 700 °C, therefore the optimum calcination temperature of 700 °C was chosen to prepare NiO-NPs.

After ensuring the successful fabrication of NiO nanoparticles at a calcination temperature of 700 °C, the catalytic activity of these nanomaterials for the synthesis of 3,4-dihydropyrano[*c*]chromenes (**4**) and 2-amino-4H-chromene derivatives (**5**) was investigated. Initially, to obtain the optimal reaction conditions, the one-pot three-component reaction of 4-Chloro benzaldehyde (1 mmol), malononitrile (1.2 mmol), and 4-hydroxycoumarin (1 mmol) were selected as a model (**4f**). The model reaction was heated in a variety of solvents such as H_2O, EtOH, CH_2Cl_2, CH_3CN, EtOH/H_2O mixture and also solvent-free condition in the presence of 20 mg of NiO-NPs (sample which calcinated at 700 °C), (Table 2, entries 1–6). It was found that the reaction gave the best result (55% yield in 60 min. when the reaction was refluxed in water, entry 1).

In the next step, the effect of the amount of catalyst and temperature on the rate and yield of the reaction was studied in water (5 ml) and observed that 20 mg of NiO-NPs at 80 °C is effective for this condensation (entry 7). The desired product also obtained an 80% yield but with a longer reaction time when using 10 mg of catalyst. Experiments showed that 20 mg of the catalyst in water (5 ml) at 80 °C for the preparation of **4f** was optimal. (Table 2, entry 7).

The scope and limitations of the reaction using optimized reaction conditions were investigated with different aromatic aldehydes. As a result, 3,4-dihydropyrano[*c*] chromene derivatives were synthesized with aromatic aldehydes containing electron-withdrawing and electron-donating substituents with good to excellent yields in relatively short reaction times, without the formation of by-products. Results are summarized in Table 3.

The catalytic activity of NiO nanoparticles was extended by the utilization of a one-pot condensation reaction from the reaction of aromatic aldehydes, malononitrile, and 1-naphthol by using 20 mg of NiO-NPs at 80 °C in water as a solvent to afford 2-amino-4H-chromene derivatives (Table 3). The obtained results showed that the reaction works well and all the reactions proceeded efficiently (Table 3, entries 8–13).

Table 2 Optimization of reaction conditions for the synthesis of 3,4-dihydropyrano[*c*]chromenes (**4f**)

Entry	Catalyst (mg)	Solvent	Temperature (°C)	Time (min)	Yield[a] (%)
1	20	H_2O	Reflux	60	55
2	20	EtOH	Reflux	60	50
3	20	CH_2Cl_2	Reflux	70	35
4	20	Solvent-free	80	90	30
5	20	H_2O:EtOH (1:1)	80	70	50
6	20	CH_3CN	80	90	Trace
7	20	H_2O	80	25	92
8	10	H_2O	80	50	80
9	30	H_2O	80	25	90
10	20	H_2O	r.t	90	Trace
11	20	H_2O	40	60	30
12	20	H_2O	60	60	50
13	Catalyst-free	H_2O	80	70	trace

Reaction conditions: 4-chlorobenzaldehyde (1 mmol), 4-hydroxycoumarin (1 mmol), and malononitrile (1.2 mmol) under different conditions

[a]Isolated yield

Figure 10 shows the proposed mechanism for the formation of 3,4-dihydropyrano[*c*]chromene derivatives by using NiO-NPs as a Lewis acid catalyst. Based on this mechanism, the activation of the C–H bond in malononitrile with O^{2-} groups of the catalyst as a Lewis base leads to the attack of malononitrile on an activated carbonyl group of aldehyde by Ni^{2+}. Then Knoevenagel condensation reaction between malononitrile and aldehyde followed by dehydration to provide the intermediate (I). Michael's addition between Intermediate (I) and 4-hydroxycoumarin further forms the intermediate (II). Then, the intramolecular cyclization and tautomerization in the presence of the catalyst result in 3,4-dihydropyrano[*c*]chromenes.

The reusability of the catalyst was investigated by employing the model reaction under optimal reaction conditions. After each run, hot ethanol was added to the reaction mixture to dissolve the product, and the catalyst was separated by filtration. The catalyst was dried at 120 °C for 2 h and then weighed to use in the model reaction under optimal conditions to prepare (**4f**). The results showed that the catalyst could be employed four times, with no significant decrease in catalytic activity, and the yields ranged from 92 to 83%. (Fig. 11).

To further confirm the stability structure and physicochemical properties of the catalyst, the XRD pattern and IR spectra of the recycled NiO-NPs catalyst were measured in comparison with that of the fresh catalyst. It was observed that no significant structural or chemical changes occurred in the NiO-NPs catalyst. These results further evidenced the robustness and stability of the nanoparticles structure of NiO under the employed reaction conditions [55] (Figs. 12 and 13).

Table 3 Synthesis of 3,4-dihydropyrano[*c*]chromene (**4**) and 2-amino-4H-chromene (**5**) derivatives using NiO-NPs
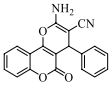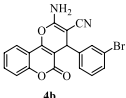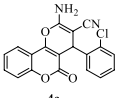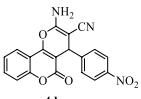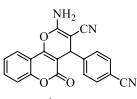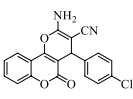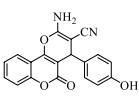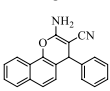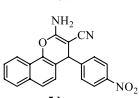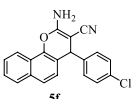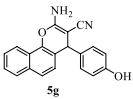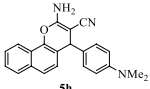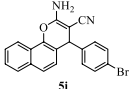
Entry	Ar	Product	Time (min)	Yield[a] (%)	M.p. (°C) Found	Reported (Refs.)
1	C$_6$H$_5$	**4a**	30	85	257–259	(256–258) [49]
2	3-Br-C$_6$H$_4$	**4b**	25	90	278–279	(272–276) [50]
3	2-Cl-C$_6$H$_4$	**4c**	25	90	267–269	(263–265) [49]
4	4-NO$_2$-C$_6$H$_4$	**4d**	10	95	257–259	(258–260) [49]
5	4-CN-C$_6$H$_4$	**4e**	10	95	282–285	(285–286) [49]
6	4-Cl-C$_6$H$_4$	**4f**	25	92	259–260	(261–262) [51]
7	4-OH-C$_6$H$_4$	**4g**	30	85	264–267	(266–268) [51]
8	C$_6$H$_5$	**5a**	30	80	210–212	(208–210) [52]
9	4-NO$_2$-C$_6$H$_4$	**5d**	30	95	235–238	(237–238) [52]
10	4-Cl-C$_6$H$_4$	**5f**	30	85	231–232	(231–233) [52]
11	4-OH-C$_6$H$_4$	**5g**	40	85	187–188	(185–187) [52]

Table 3 (continued)

Entry	Ar	Product	Time (min)	Yield[a] (%)	M.p. (°C) Found	Reported (Refs.)
12	4-NMe$_2$-C$_6$H$_4$	**5h**	45	85	200–202	(201–203) [53]
13	4-Br-C$_6$H$_4$	**5i**	30	92	232–235	(234–236) [54]

Reaction conditions: aldehyde (1 mmol), malononitrile (1.2 mmol), 4-hydroxycoumarin / 1-naphthol (1 mmol), H$_2$O (5 mL), NiO-NPs (0.02 g) and 80 °C. All products were characterized by a comparison of their spectral and physiochemical characteristics with those of the authentic samples synthesized by published procedures
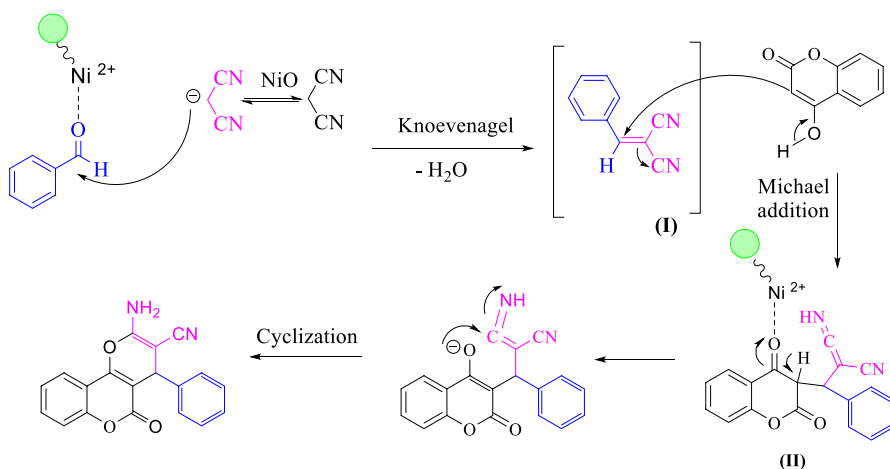
[a]Isolated yield

Fig. 10 A probable mechanism for the synthesis of 3,4-dihydropyrano[*c*]chromenes using NiO-NPs

Also, to show the advantages of this method, the efficiency of the present catalyst was compared with some reported catalysts for the synthesis of 3,4- dihydropyrano[c] chromenes. As shown in Table 4, NiO nanoparticles are comparable with most of the reported catalysts in terms of yield, reaction time, and reaction conditions. Moreover, the present catalyst is superior due to biosynthesis and recyclability.
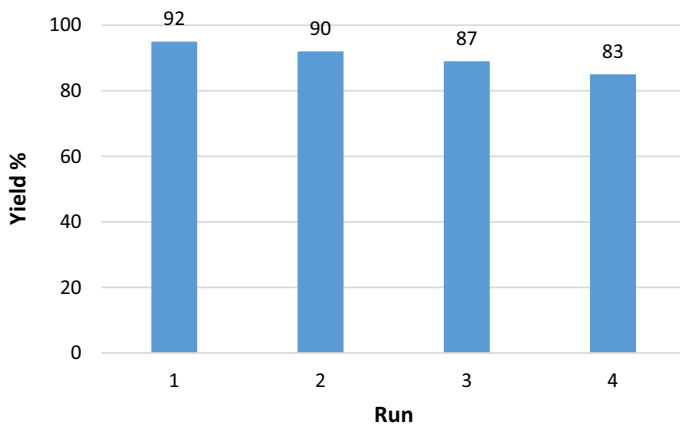
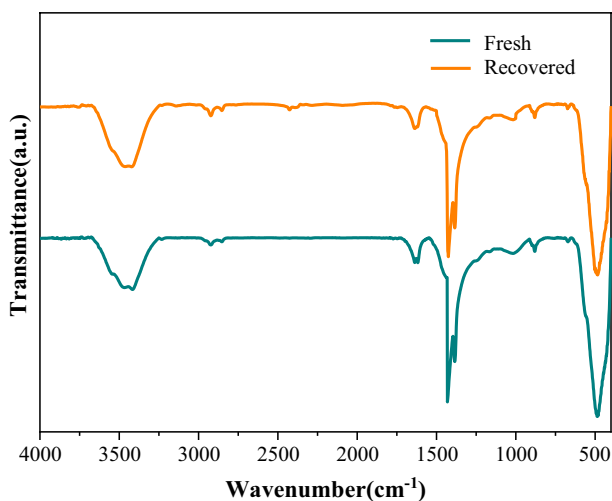**Fig. 11** Reusability of the catalyst in the model Reaction

Fig. 12 FT-IR spectra of NiO-NPs synthesized using mucilage of *Cordia myxa* (fresh and recovered)

Conclusion

In this research, NiO nanoparticles were synthesized for the first time, using mucilage of *Cordia myxa* fruit by sol–gel method at different calcination temperatures (500, 600, and 700 °C). The XRD results show that increasing the calcination temperature increases the intensity of crystallinity, although the average particle size also increases. FT-IR results confirm the formation of NiO nanoparticles with a strong absorption band in the region of 420–500 cm^{-1} in all samples. The use of a mucilage template led to the synthesis of particles with nanometer dimensions (15 to 27 nm).
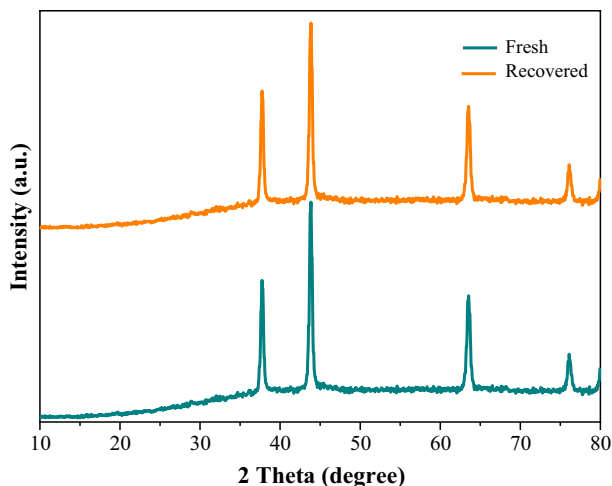
Fig. 13 XRD patterns of NiO–NPs synthesized using mucilage of *Cordia myxa* (fresh and recovered)

Table 4 Comparison of catalytic activity of NiO-NPs with some other catalysts for the synthesis of (**4f**)

Entry	Catalyst	Solvent	Temp. (℃)	Time (min)	Yield (%)	References
1	S-proline		r.t	120	81	[56]
2	$H_6P_2W_{18}O_{62}$–$18H_2O$	H_2O: EtOH (1:1)	reflux	30	89	[57]
3	$(CH_2)_6N_4$	EtOH	Reflux	15	92	[58]
4	Nano ZnO	H_2O	70	180	87	[39]
5	CuO nanoparticles	H_2O	r.t	6	93	[38]
6	Thiourea dioxide (TUD)	H_2O	70	13	93	[51]
7	Nano $CuCr_2O_4$	H_2O	r.t	6	88	[49]
8	OBS	Solvent-free	120	50	85	[59]
9	Ni (II)-Schiff base/SBA-15	H_2O	70	10–15	95	[36]
10	NH_4OAc	Bmim[triflate]	r.t or100	50	94	[60]
11	Fe_3O_4@SiO_2-Imine/Phenoxy-Cu(II)	Solvent-free	90	17	95	[50]
12	NiO-NPs	H_2O	80	25	92	This work

According to the use of the green method in this research, the catalytic activity of nickel oxide synthesized at 700 temperature in the synthesis of 3,4-dihydropyrano[*c*]chromenes and 2-amino-4H-chromene derivatives was investigated. The set of this method includes single-step, use of non-toxic catalyst, and environmentally friendly conditions. All products were identified by FT-IR, ^{1}H-NMR, and ^{13}C-NMR spectroscopy and melting points which were compared with reported compounds. In the end, the catalyst was easily recovered from the reaction medium and could be reused several times in a row.

Declarations

Conflict of interest The authors declare no competing interests.

Ethical approval The current study does not contain any studies with human or animal subjects.

References

1. Y. Mbenga, M.N. Mthiyane, T.L. Botha, S. Horn, R. Pieters, V. Wepener, D.C. Onwudiwe, J. Inorg. Organomet. Polym. **32**, 3249 (2022)
2. A. Angel Ezhilarasi, J. Judith Vijaya, K. Kaviyarasu, L. John Kennedy, R. Jothiramalingam, H.A. Al-Lohedan, J. Photochem. Photobiol. B Biol. **180**, 39 (2018)
3. Z. Sabouri, N. Fereydouni, A. Akbari, H.A. Hosseini, A. Hashemzadeh, M.S. Amiri, R. Kazemi Oskuee, M. Darroudi, Rare Met. **39**, 1134 (2020)
4. A. Haider, M. Ijaz, S. Ali, J. Haider, M. Imran, H. Majeed, I. Shahzadi, M. Muddassir Ali, J. Ali Khan, M. Ikram, Nanoscale Res. Lett. **15**, 50 (2020)
5. S. Ghazal, A. Akbari, H.A. Hosseini, Z. Sabouri, F. Forouzanfar, M. Khatami, M. Darroudi, J. Mol. Struct. **1217**, 128378 (2020)
6. F. Liu, Y. Sang, H. Ma, Z. Li, Z. Gao, J. Nat. Gas Sci. Eng. **41**, 1 (2017)
7. A.A. Ezhilarasi, J.J. Vijaya, K. Kaviyarasu, M. Maaza, A. Ayeshamariam, L.J. Kennedy, J. Photochem. Photobiol. B **164**, 352 (2016)
8. M. Hafeez, R. Shaheen, B. Akram, Zain-ul-Abdin, S. Haq, S. Mahsud, S.H. Ali, R. Taj Khan, Mater. Res. Express **7**, 025019 (2020)
9. K. Kombaiah, J. Judith Vijaya, L. John Kennedy, M. Bououdina, R. Jothi Ramalingam, H.A. Al-Lohedan, Mater. Chem. Phys. **204**, 410 (2018)
10. S.A. Prisrin, M. Priyanga, K.M. Ponve, K. Kaviarasan, S. Kalidass, J. Clust. Sci. **33**, 765 (2022)
11. I. Bibi, N. Nazar, M. Iqbal, S. Kamal, H. Nawaz, S. Nouren, F.Y. Safa, K. Jilani, M. Sultan, S. Ata, F. Rehman, M. Abbas, Adv. Powder Technol. **28**, 2035 (2017)
12. A. Indriyani, Y. Yulizar, R.T. Yunarti, D.O. Bagus Apriandanu, R. Marcony Surya, Appl. Surf. Sci. **563**, 150113 (2021)
13. Y. Yulizar, D.O. Sudirman, J. Bagus Apriandanu, L. Al Jabbar, Inorg. Chem. Commun. **123**, 108320 (2021)
14. R. Marcony Surya, S. Mauliddiyah, D.O. Bagus Apriandanu, Sudirman, Y. Yulizar, Chemosphere **304**, 135125 (2022)
15. M.S. Amiri, V. Mohammadzadeh, M.E. Taghavizadeh Yazdi, M. Barani, A. Rahdar, G.Z. Kyzas, Molecules **26**, 1770 (2021)
16. G. Goksen, D. Demir, K. Dhama, M. Kumar, P. Shao, F. Xie, N. Echegaray, J.M. Lorenzo, Int. J. Biol. Macromol. **230**, 123146 (2023)
17. S. Ghazal, N. Khandannasab, H.A. Hosseini, Z. Sabouri, A. Rangrazi, M. Darroudi, Ceram. Int. **47**(19), 27167 (2021)
18. L. Hernandez-Morales, H. Espinoza-Gomez, L.Z. Flores-Lopez, E.L. Sotelo-Barrera, A. Nunez-Rivera, R.D. Cadena-Nava, G. Alonso-Nunez, K.A. Espinoza, Appl. Surf. Sci. **489**, 952 (2019)
19. Z. Sabouri, A. Rangrazi, M.S. Amiri, M. Khatami, M. Darroudi, Bioprocess Biosyst. Eng. **44**, 2407 (2021)

20. S. Ghazal, A. Akbari, H.A. Hosseini, Z. Sabouri, F. Forouzanfar, M. Khatami, M. Darroudi, Appl. Phys. A **126**, 480 (2020)
21. F.N. Eze, C. Ovatlarnporn, T.J. Jayeoye, S. Nalinbenjapun, S. Sripetthong, Int. J. Biol. Macromol. **206**, 521 (2022)
22. Z. Sabouri, A. Akbari, H.A. Hosseini, M. Khatami, M. Darroudi, Green Chem. Lett. Rev. **14**, 402 (2021)
23. C. Engelbrekt, K.H. Sørensen, J. Zhang, A.C. Welinder, P.S. Jensen, J. Ulstrup, J. Mater. Chem. **19**, 7839 (2009)
24. H. Elhosiny Ali, M.M. Abdel-Aziz, A.M. Aboraia, I.S. Yahia, H. Algarni, V. Butova, A.V. Soldatov, Y. Khairy, Optik **227**, 165969 (2021)
25. S.M. Yakout, A.A. Mostafa, Int. J. Clin. Exp. Med. **8**, 3538 (2015)
26. B. Ankamwar, M. Salgaonkar, U. Kumar Sur, Inorg. Nano-Met. Chem. **47**(9), 1359 (2017)
27. S. Batool, M. Hasan, M. Dilshad, A. Zafar, T. Tariq, Z. Wu, R. Chen, S.G. Hassan, T. Munawar, F. Iqbal, M.S. Saif, M. Waqas, X. Shu, Adv. Powder Technol. **33**, 103780 (2022)
28. S. Keshani Dokht, Z. Emam Djomeh, M.S. Yarmand, M. Fathi, Int. J. Biol. Macromol. **118**, 485 (2018)
29. M. Heilmann, H. Kulla, C. Prinz, R. Bienert, U. Reinholz, A. Guilherme Buzanich, F. Emmerling, Nanomaterials **10**, 713 (2020)
30. J. Safaei-Ghomi, F. Eshtegha, M.A. Ghasemzadeh, Acta Chim. Slov. **61**, 703 (2014)
31. T. Shamsi, A. Amoozadeh, S.M. Sajjadi, E. Tabrizian, Appl. Organomet. Chem. **31**, e3618 (2017)
32. D.S. Patel, J.R. Avalani, D.K. Raval, J. Saudi Chem. Soc. **20**, S401 (2016)
33. S. Jain, D. Rajguru, B.S. Keshwal, A.D. Acharya, Int. Sch. Res. Not. **2013**, 185120 (2016)
34. B. Shitole, N. Shitole, M. Shingare, G. Kakde, Curr. Chem. Lett. **5**, 137 (2016)
35. E. Jahangard, L. Khazdooz, A. Zarei, Iran. J. Catal. **10**(1), 57 (2020)
36. N. Noroozi Pesyan, G. Rezanejade Bardajee, E. Kashani, M. Mohammadi, H. Batmani, Res. Chem. Intermed. **46**, 347 (2020)
37. M. Seifi, H. Sheibani, Catal. Lett. **126**, 275 (2008)
38. H. Mehrabi, M. Kazemi-Mireki, Chin. Chem. Lett. **22**, 1419 (2011)
39. S. Paul, P. Bhattacharyya, A.R. Das, Tetrahedron Lett. **52**, 4636 (2011)
40. V. Selvanathan, M. Shahinuzzaman, S. Selvanathan, D. Kumar Sarkar, N. Algethami, H.I. Alkhammash, F.H. Anuar, Z. Zainuddin, M. Aminuzzaman, H. Abdullah, M.D. Akhtaruzzaman, Catalysts **11**(12), 1523 (2021)
41. D.O. Bagus Apriandanu, Y. Yulizar, Nano-Struct. Nano-Objects **20**, 100401 (2019)
42. V.K. Sharma, B. Mazumdar, Ind. Crops Prod. **50**, 776 (2013)
43. M. Anvari, M. Tabarsa, R. Cao, S. You, H.S. Joyner (Melito), S. Behnam, M. Rezaei, Food Hydrocolloid **52**, 766 (2016)
44. Z. Sabouri, A. Akbari, H.A. Hosseini, A. Hashemzadeh, M. Darroudi, J. Clust. Sci. **30**, 1425 (2019)
45. P. Karpagavinayagam, A. Emi Princess Prasanna, C. Vedhi, Mater. Today Proc. **48**, 136 (2022)
46. H.A. Ariyanta, T.A. Ivandini, Y. Yulizar, J. Mol. Struct. **1227**, 29543 (2021)
47. M. Iqbal, A. Haq, G. Antonio Cerrón-Calle, S.A.Z. Naqvi, P. Westerhoff, S. Garcia-Segura, Catalysts **11**(7), 806 (2021)
48. K.N. Patel, M.P. Deshpande, K. Chauhan, P. Rajput, V.P. Gujarati, S. Pandya, V. Sathe, S.H. Chaki, Adv. Powder Technol. **29**, 2394 (2018)
49. Z. Karimi-Jaberi, M.S. Moaddeli, M. Setoodehkhah, M.R. Nazarifar, Res. Chem. Intermed. **42**, 4641 (2016)
50. M. Nesarvand, D. Azarifar, H. Ebrahimiasl, Res. Chem. Intermed. **47**, 3629 (2021)
51. S.S. Mansoor, K. Logaiya, K. Aswin, P. Nithiya Sudhan, J. Taibah Univ. Sci. **9**, 213 (2015)
52. S.V. Goswami, S.S. Pendalwar, S.R. Bhusare, Chem. Biol. Interface **6**, 171 (2016)
53. M.R. Poor Heravi, M.R. Amirloo, Chem. Commun. **3**, 62 (2015)
54. M.G. Dekamin, M. Eslami, A. Maleki, Tetrahedron **69**, 1074 (2013)
55. T. Quang-Hung, T.T. Do, V.Q. Hoang, D.M. Tran, N. Quoc-Anh, T.-A.L. Hoang, R. Eckelt, D.V. Do, T.T. Dang, X.-H. Vu, Chem. Pap. **77**, 89 (2023)
56. S. Abdolmohammadi, S. Balalaie, Tetrahedron Lett. **48**, 3299 (2007)
57. M. Heravi, B. Alimadadi Jani, F. Derikvand, F. Bamoharram, H.A. Oskooie, Catal. Commun. **10**, 272 (2008)
58. H. Juan Wang, J. Lu, Z.H. Zhang, Monatsh. Chem. **141**, 1107 (2010)
59. B. Maleki, Org. Prep. Proced Int. **48**, 303 (2016)

60. M. Chiheb, B. Lamia, T. Riadh, M. Lamjed, H. Abdel Halim, J. Al-Tamimi, B. Lassaad, H. Naceur, J. Heterocycl. Chem. **57**, 291 (2020)